Welding in the World, Volume 68, June 2024, pp. 1389-1399
DOI: 10.1007/s40194-023-01668-3

Enhancing Microstructural and Mechanical Characteristics of Laser Welded NiTi SMA/304 SS Lap Joints with Medium and High Entropy Alloy Fillers

Wang Yipeng[1], Zhang Dongni[2*], Li Hong[1*], Li Zhuoxin[1], Yang Zijia[3], Chen Xin[4], Cong Baoqiang[5]
[1]Department of Materials Science and Engineering, Faculty of Materials and Manufacturing, Beijing University of Technology, Beijing 100124, China
[2]Science and Technology on Power Beam Processes Laboratory, AVIC Manufacturing Acturing Technology Institute, Beijing 100024, China
[3]Harbin Welding Institute Co.,Ltd., Harbin 150028, China
[4]Welding and Additive Manufacturing Centre, Cranfield University, Bedfordshire MK43 0AL, UK
[5]School of Mechanical Engineering and Automation, Beihang University, Beijing 100191, China
*Corresponding authors, email: dongni_zhang@126.com (Zhang Dongni); hongli@bjut.edu.cn (Li Hong)

Abstract: The demand for high-quality nickel-titanium (NiTi) shape memory alloy (SMA) and stainless steel (SS) welded structures has led to significant challenges in fusion welding technology, which is largely influenced by filler materials. This study explores the application of CoCrNi medium entropy alloy and CoCrNiFe high entropy alloy as filler materials for laser lap welding of NiTi SMA and 304 SS. A self-fusing joint was produced for comparison. The results demonstrate that the interface zone on the NiTi side was the weakest area regarding cracking defects in NiTi/304 SS lap joints. However, using CoCrNi and CoCrNiFe fillers effectively eliminated cracking defects by considerably suppressing the formation of brittle FeTi and Fe_2Ti intermetallic compounds (IMCs). The average microhardness value of the weld zone without filler was higher than with CoCrNi and CoCrNiFe. Furthermore, the addition of CoCrNi and CoCrNiFe fillers to NiTi/304 SS lap joints resulted in a substantial increase in tensile properties, with tensile strength reaching 196±39 MPa without filler, 319±25 MPa with CoCrNi, and 377±33 MPa with CoCrNiFe respectively.

Keywords: Nickel-titanium shape memory alloy; Stainless steel; medium entropy alloy; high entropy alloy; laser welding

1. Introduction

As an important functional material, the nickel-titanium (NiTi) alloy holds great promise in various fields, including biomedical, aerospace, and communications, due to its unique properties, such as shape memory effect, super-elasticity, corrosion resistance, and biocompatibility [1,2]. However, the

Published by Springer. This is the Author Accepted Manuscript.
The final published version (version of record) is available online at DOI:10.1007/s40194-023-01668-3. Please refer to any applicable publisher terms of use.

high cost, low yield strength, and simplistic structure of NiTi shape memory alloy (SMA) products restrict their broader application[3,4]. To overcome these limitations, combining NiTi with other materials can create multi-material systems that leverage the beneficial properties of each component. Stainless steel (SS), with its low cost, high specific strength, good machinability, and biocompatibility, represents an ideal candidate to compensate for NiTi's drawbacks, especially in fabricating complex components for biomedical applications [5]. Therefore, the demand for joining NiTi and SS is significant, and achieving high-quality NiTi/SS joints has become a formidable challenge [6].

At present, various welding processes are available for joining NiTi and SS, including spot welding [7,8], Tungsten Inert Gas (TIG) welding [9], electron beam welding [10], and laser beam welding. Among these, laser welding is the most commonly adopted process due to its advantages of high energy density, narrow heat-affected zone (HAZ), and minimal weld distortion. Although a highly controllable heat source is employed, laser welding of NiTi to SS still faces a serious challenge, namely the formation of hard and brittle intermetallic compounds (IMCs), in particular Ti-Fe phases, which is difficult to suppress because NiTi and SS have similar melting points (NiTi: 1583 K, SS: ~1673 K) and their melting and mixing are usually unavoidable when welded directly [11]. The precipitation of IMCs can lead to weld defects such as microcracks and macrosegregation, adversely affecting the performance of NiTi/SS welded joints [12].

To improve the quality of NiTi/SS welded structure, substantial research work has been carried out based on the concept of eliminating brittle intermetallic compounds by introducing intermediate filler materials between two base metals. C.H. et al., [13] applied the high-melting-point metal Ta as an interlayer foil in the laser welding of NiTi to AISI 316L SS. They identified that the presence of Ta interlayer played a role as a diffusion barrier between NiTi and SS, thus restricting the formation of Ti-Fe IMCs and improving the joint tensile strength. Filler materials such as Cu [14], Co [15], and Ni [16] were also employed for the joining of NiTi and SS respectively. Similar findings were observed that the joint mechanical properties were enhanced to some extent by changing the weld chemical composition and forming favorable intermetallic compounds such as Ni_3Ti and γ phase, which were more ductile than the Ti-Fe phases. However, a common problem in the above studies is that the amount of the filler materials must be strictly controlled, as excessive addition of them can lead to the formation of other harmful IMCs like Cr_2Ta and Ni_3Ta for Ta filler, Ti-Cu IMCs for Cu filler and Ti-Co IMCs for Co filler, which will in turn deteriorate the joint properties [17]. Therefore, it is still necessary to explore

a more appropriate filler material that can improve the NiTi/SS joint performance without generating harmful IMCs.

High entropy alloy (HEA) has recently attracted extensive attention due to its superior mechanical properties [18]. HEA is based on a multi-principal-component alloying system and demonstrates high entropy, meaning that the elements prefer to distribute randomly in a lattice to form a solid solution rather than complex phases or IMCs [19,20,21]. Different challenging dissimilar metals, including aluminium alloy/steel [22], titanium/aluminium alloys [23], magnesium/aluminium alloys [24], and SMA490BW steel/304 stainless steel [25], have been successfully joined by using various HEAs as the filler materials. As a representative HEA, CoCrFeNiMn alloy, also known as Cantor alloy, whose microstructure is a face-centered cubic (FCC) (Fe, Ni) solid solution, exhibits an excellent combination of high strength and ductility. Wang et al., [26] used CoCrFeNiMn as a filler material for the joining of NiTi/SS dissimilar alloys. It was revealed that the introduction of CoCrFeMnNi significantly reduced the formation of Fe-Ti intermetallic compounds and enhanced the (Fe, Ni) solid solution and B2 phases, leading to improved mechanical properties of the NiTi/SS welded joint.

Recent research has shown that there is no direct correlation between the number of alloying elements and the mechanical properties of multi-principal-component alloys [27,28]. The derivatives of Cantor alloy like three-principal-component CoCrNi medium-entropy alloy (MEA) and four-principal-component CoCrNiFe HEA have been reported to present a better combination of strength and ductility compared to five-principal-component CoCrFeNiMn HEA, which was attributed to the solid solution strengthening caused by severe local lattice distortion [29,30,31]. This finding indicates that CoCrNi and CoCrNiFe fillers have great potential in the joining of NiTi and SS dissimilar metals. However, no relevant work has been reported, and the influence of CoCrNi and CoCrNiFe on the joining of NiTi and SS remains unclear.

The present study aims to explore the effects of CoCrNi MEA and CoCrNiFe HEA on the microstructure and mechanical properties of NiTi/SS welded joints. Laser welding process was employed to produce the NiTi/SS lap joints. A NiTi/SS joint without filler was also fabricated using the same process parameters for comparative analysis. The results of this study will provide valuable experimental data for achieving high-quality joining of NiTi and SS using medium and high entropy alloys as filler materials.

2. Materials and experimental procedure

Nickel-titanium shape memory alloy and 304 stainless steel were employed as the base metals, with their chemical compositions listed in **Table 1** and **Table 2**, respectively. The dimensions of both materials were 120 mm× 45 mm× 1.5 mm. Three-component CoCrNi MEA made from equal molar ratio Co, Cr and Ni powders, and four-component CoCrNiFe HEA made from equal molar ratio Co, Cr, Ni and Fe powders were used as filler materials, respectively. The powders were prepared in sizes from 45 to 105 microns by vacuum atomization method, and their SEM images are shown in **Fig. 1**.

Table 1 Chemical composition of NiTi SMA (wt.%)

Material	Ni	C	O	N	Ti
NiTi SMA	56.870	0.040	0.051	0.005	43.034

Table 2 Chemical composition of 304 SS (wt.%)

Material	C	Si	Mn	Cr	Ni	S	P	Fe
304 SS	≤0.07	≤1.0	≤2.0	17.0~19.0	8.0~11.0	≤0.03	≤0.035	Balance

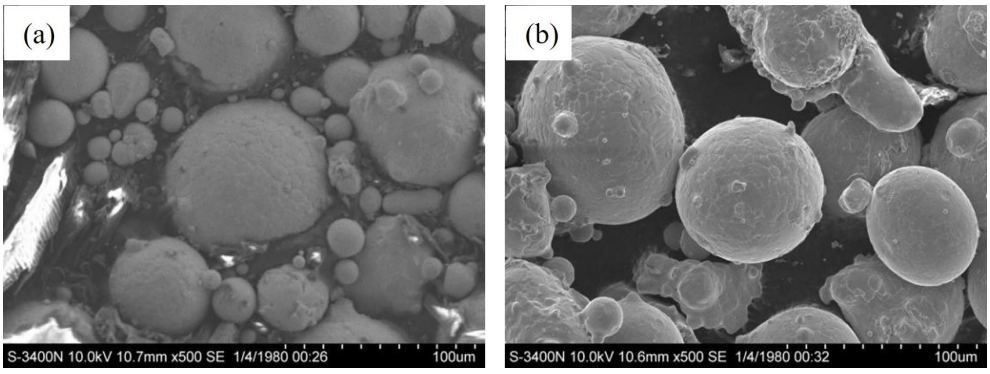

Fig. 1 Morphology of the filler materials. (a) CoCrNi; (b) CoCrNiFe.

As demonstrated in **Fig. 2**, the laser welding system primarily consisted of a YLS-4000 type fiber laser source with a maximum output power of 4000W (adjustable within the range of 10-100%), a wavelength of 1070±10 nm, a focal length of 200 mm, and a minimum beam diameter of 0.2 mm. A BIMO series laser head with a maximum output power of 6000W and a KUKA-KR60 type welding robot were used. CoCrNi and CoCrNiFe powders were employed as filler materials for laser lap welding of NiTi and 304 SS. For comparison, a self-fusing joint was also produced. Before welding, the workpieces were prepared by grinding with an angle grinder to remove surface contaminants. They were then cleaned using the ultrasonic vibration method in acetone solution and further cleaned with alcohol to eliminate oil stains. As schematically illustrated in **Fig. 3**, to minimize the impact of heat input on the shape memory effect, the NiTi sheet was placed at the bottom, and the 304 SS sheet was

placed on top, both securely held in place with jigs on the sides, with 3mm overlap length. 9 g of the two powders were weighted accurately and evenly spread at the corner between the two workpieces respectively. The laser beam was directed at a 30-degree angle to the vertical direction and focused on the powders. Based on preliminary experiments, the optimal process parameters were determined to achieve joints without significant formation defects. These parameters included a laser power of 1500W, a laser beam diameter of 2 mm, a 1 m/min welding speed, and a shielding gas (99.99% argon) flow rate of 25 L/min.

Fig. 2 Laser welding system for the experiments.

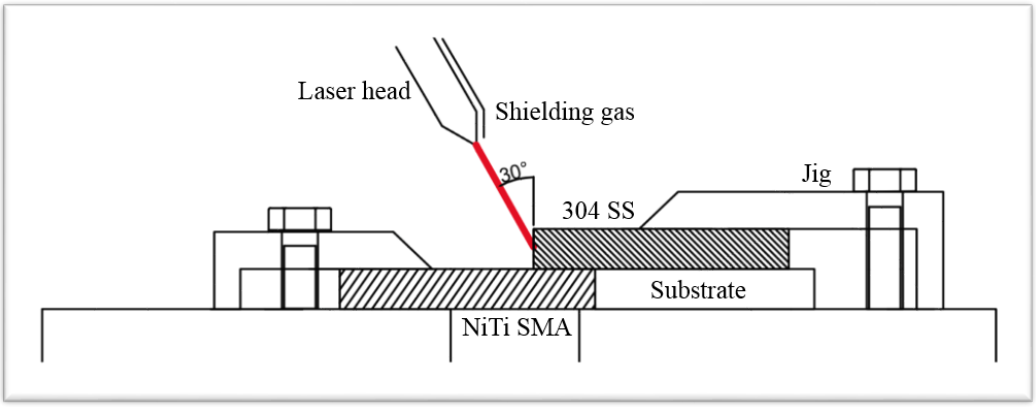

Fig. 3 Schematic illustration of NiTi /304 SS laser lap welding.

The samples used for microstructure observation and mechanical properties testing were extracted from the middle of the workpieces. Microstructure observation was conducted using a SU8020-type scanning electron microscope (SEM), and component analysis was performed using energy dispersive spectrometry (EDS) equipped with the SEM. Phase analysis was carried out using an AD8 Advance-type X-ray diffractometer. Electron back-scattered diffraction (EBSD) testing was employed for grain

size statistics and grain orientation analysis. Micro hardness testing was performed using a MICRO MET-5103 type digital Vickers (HV) hardness tester, with a loading force set to 0.981 N and a duration time of 10 seconds. As illustrated in **Fig. 4**a, the test points were evenly distributed along the centerline between the parent metal and the weld bead. For the tensile property test, specimens with dimensions shown in **Fig. 4**b were used. The tensile shear test was conducted at ambient temperature using a CMT5504-type electronic universal testing machine with a 1 mm/min loading rate.

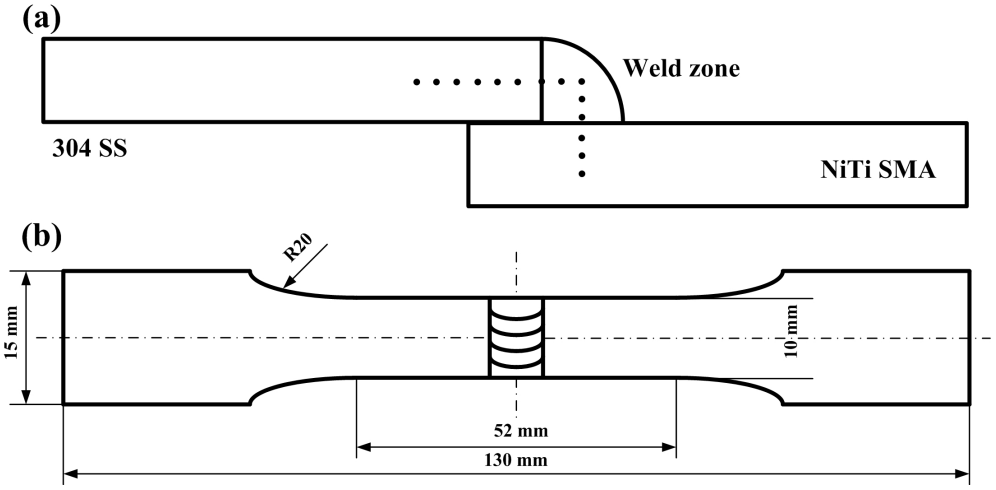

Fig. 4 Diagram of specimens for mechanical property test. (a): Micro hardness; (b): Tensile shear property.

3. Results and discussion

3.1 Cracking formation

Fig. 5 displays SEM images showing the macroscopic view of NiTi/304 SS lap joints with different fillers. For the joint without filler in **Fig. 5a**, large-scale primary cracks can be observed penetrating the weld zone and extending into the interface zone on the NiTi side. Several secondary cracks appeared in the interface zone, propagating through and along the boundary of the bright white phases. In contrast, the joints with CoCrNi and CoCrNiFe fillers in **Fig. 5b** and **Fig. 5c**, respectively, showed no cracks in the weld zone. For the joint with CoCrNi filler, only a microcrack was formed in the interface zone on the NiTi side, propagating along the fusion line. The joint with CoCrNiFe filler exhibited a similar crack distribution pattern, with additional microcracks forming in the interface zone on the NiTi side. These results indicate that the weakest area of the NiTi/304 SS lap joints in terms of cracking defects is the interface zone on the NiTi side, which is in agreement with the findings when using other filler materials

such as CoCrNiFeMn HEA and Ni as filler materials [10,26]. Moreover, CoCrNi and CoCrNiFe fillers can significantly reduce the cracking susceptibility of the joint compared to that without a filler.

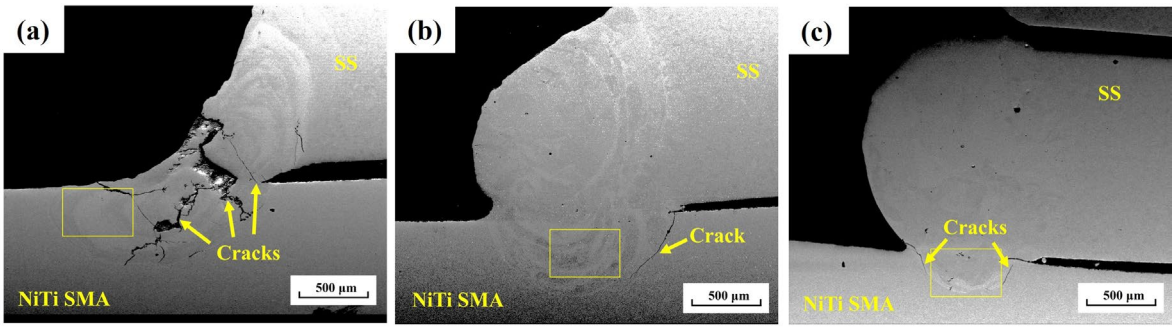

Fig. 5 Macrostructure of NiTi/304 SS lap joints with different fillers. (a): Without filler; (b): CoCrNi; (c): CoCrNiFe.

3.2 Microstructure

To explore the microstructural and phase composition variations in NiTi/304 SS lap joints with different fillers, SEM observation, and EDS detection were conducted specifically at the interface zones on the NiTi side, denoted by the yellow square in **Fig. 5**. The results (**Fig. 6**) showed that all three joints exhibited continuously distributed island-like bright white phases. Wang et al., [26] previously demonstrated that this island macro segregation in laser-welded NiTi/304 SS joints is primarily caused by the inward Marangoni convection of the molten pool and the rapid solidification process. Compared with the joint without filler, the size of the bright phases was much smaller, and their distribution was more dispersed in the joints with CoCrNi and CoCrNiFe filler.

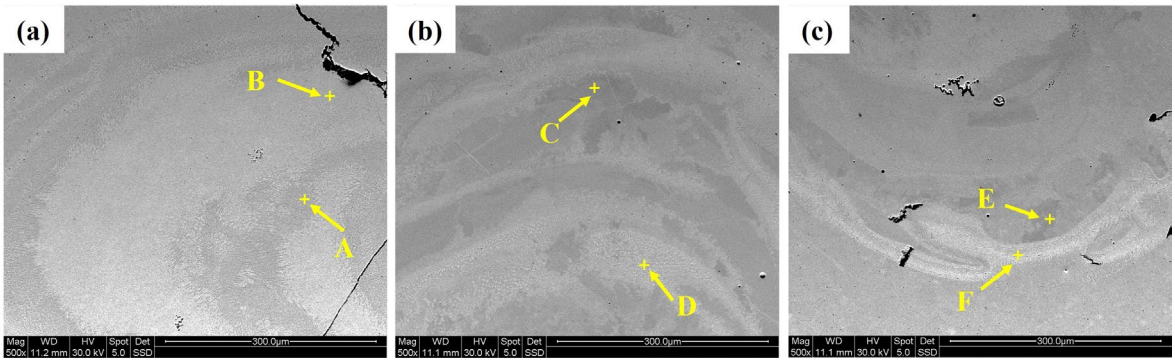

Fig. 6 SEM images of the interface zones on the NiTi side with different fillers. (a): Without filler; (b): CoCrNi; (c): CoCrNiFe.

The element composition of the tested points in **Fig. 6** was analyzed using EDS, and the results are presented in **Table 3**. By comparing the element composition of points B, D, and F, which represent the bright phases in the interface zone on the NiTi side, it is evident that the joint without filler had the

highest Fe content, followed by the joint with CoCrNiFe, and the joint with CoCrNi had the lowest Fe content. This observation is further supported by the results of EDS element mapping, as shown in **Fig. 7**. The higher Fe content on the NiTi side in the joint without filler indicates a greater potential for the formation of Fe_2Ti and FeTi intermetallic compounds, which can significantly influence the cracking susceptibility. In contrast, the joints with CoCrNi and CoCrNiFe fillers exhibited a remarkable reduction in Fe element on the NiTi side. This reduction can be attributed to the sluggish diffusion effect, a characteristic feature of high entropy alloys [32], which effectively hinders the diffusion of elements between NiTi and 304 SS.

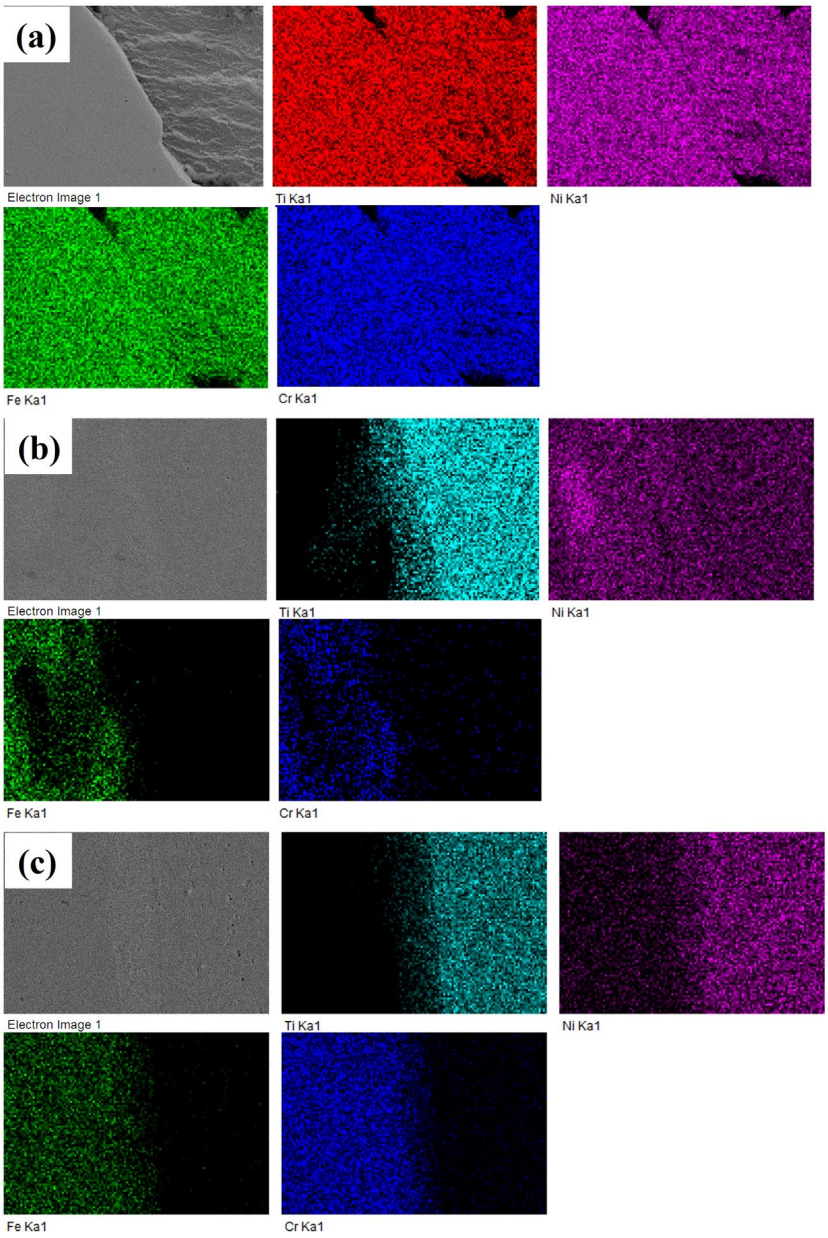

Fig. 7 EDS element mapping of the interface zones on the NiTi side with different fillers. (a): Without filler; (b): CoCrNi; (c): CoCrNiFe.

Table 3 EDS results of the tested points (at.%)

Point	Fe	Ni	Ti	Cr	Co
A	40.94	28.05	18.85	12.17	-
B	40.38	28.38	20.81	10.42	-
C	29.65	25.09	7.02	23.69	14.56
D	17.41	33.6	19.78	16.24	12.98
E	42.23	18.72	2.37	22.5	14.18
F	21.61	29.15	28.73	12.16	8.35

In conjunction with the EDS analysis and XRD pattern results in **Fig. 8**, the joint without filler primarily consisted of FeTi and Fe_2Ti intermetallic compounds (IMCs), and (Fe, Ni) solid solutions. However, when CoCrNi and CoCrNiFe were used as filler materials, the formation of FeTi and Fe_2Ti IMCs was significantly inhibited. Instead, a considerable amount of relatively ductile phases, including (Fe, Ni) solid solutions, Ni-Fe, and Cr-Ti compounds, were observed, which is believed to be attributed to the high entropy effect. An increase in the entropy of the alloys was paralleled by an increased probability of forming simply structured solid solutions, subsequently reducing the formation of IMCs [26]. In essence, the addition of CoCrNi and CoCrNiFe to NiTi/304 SS welded joints plays a crucial role in suppressing the formation of brittle FeTi and Fe_2Ti IMCs. This, in turn, promotes the generation of ductile (Fe, Ni) solid solutions.

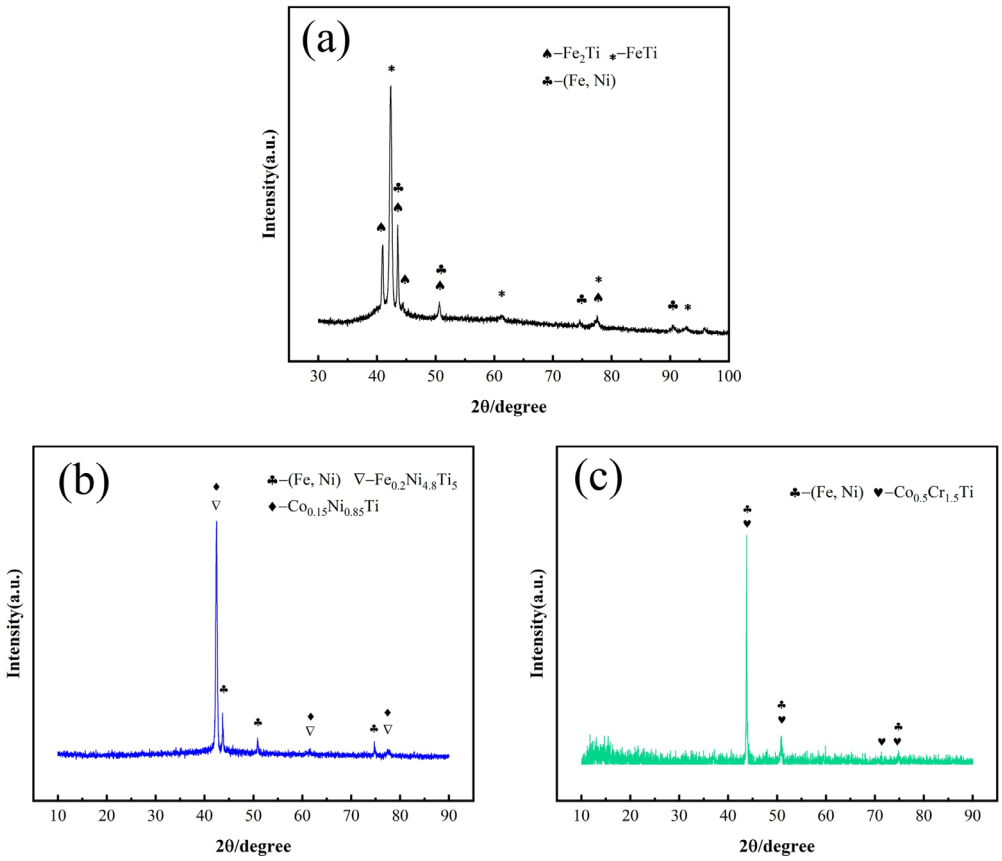

Fig. 8 XRD patterns of NiTi/304 SS lap joints with different fillers. (a): Without filler; (b): CoCrNi; (c): CoCrNiFe.

EBSD grain size mappings and statistical distribution of grain size in the interface zones on the NiTi side with CoCrNi and CoCrNiFe fillers are shown in **Fig. 9**. Note that the grain morphology characteristics in the joint without filler were not discussed due to its serious cracking defects. According to the statistical results, the average grain size of the interface zone with CoCrNi filler was 54.4 μm, and it was 93.4 μm with CoCrNiFe filler, which indicated that the grain structure in the interface zone was significantly refined when CoCrNi filler was used. **Fig. 10** illustrates the EBSD grain boundary mapping and statistical grain misorientation angle distribution. The average grain misorientation angle was 36.1° with CoCrNi and 32.9 ° with CoCrNiFe fillers. The grain misorientation angle with CoCrNi was 10% higher than that with CoCrNiFe. Additionally, the number fraction of low-angle grain boundaries (LAGB) was 19.6% with CoCrNi, but 24.8% with CoCrNiFe, suggesting that the density of LAGB in the interface zone with CoCrNi was significantly reduced compared to that with CoCrNiFe.

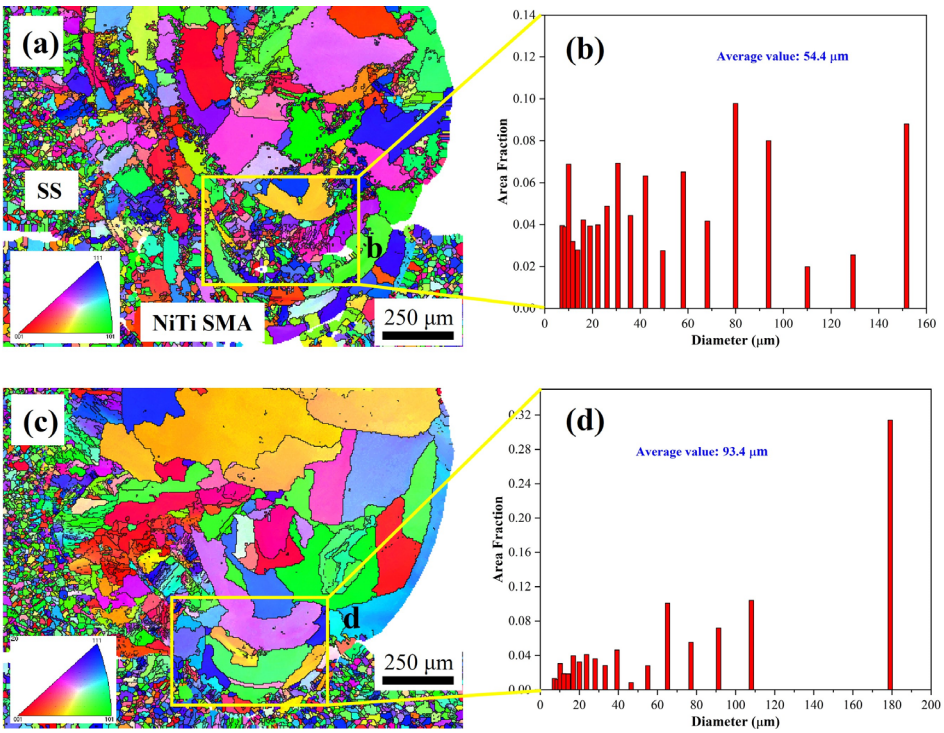

Fig. 9 EBSD IPF mapping and statistical results of the interface zones on the NiTi side with different fillers. (a) and (b): CoCrNi; (c) and (d): CoCrNiFe.

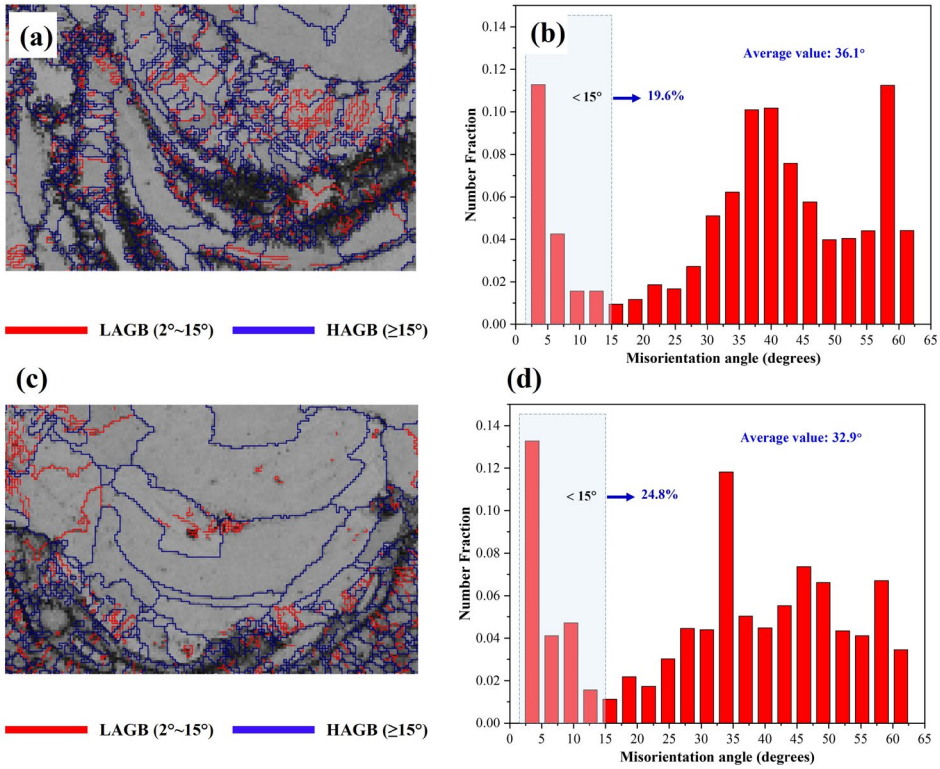

Fig. 10 EBSD grain boundary mapping and statistical results of grain misorientation angle distribution of the interface zone on the NiTi side with different fillers. (a) and (b): CoCrNi; (c) and (d): CoCrNiFe.

Since there is a significant difference in the coefficient of linear expansion between NiTi (10×10^{-6}/K) and 304 SS (17.2×10^{-6}/K), the residual stress in NiTi/304 SS lap joints will be at a high level after the fusion welding process of rapid melting and solidification [26]. For the joint without filler, the microstructure shows a large number of continuously distributed large-scale Fe-Ti IMCs, characterized by hard and high brittle, in the weld zone, partially on the NiTi side. As a result, the cracks originate from the weld zone center and propagate heavily to the interface on the NiTi side. For the condition that CoCrNi MEA and CoCrNiFe HEA are introduced as the filler materials, the type of IMCs change to relatively ductile (Fe, Ni) solid solutions, Ni-Fe, and Cr-Ti compounds, which is beneficial to reduce the initiation of cracks. Moreover, the relatively dispersive distribution of these phases in the interface zone on the NiTi side plays a role in blocking the propagation of cracks. These results in the effective suppression of cracks in the laser-welded NiTi/304 SS lap joints by CoCrNi and CoCrNiFe fillers.

3.3 Microhardness

Fig. 11 displays the microhardness distribution of NiTi/304 SS lap joints with different fillers. In the joint without filler, the average microhardness values of both NiTi (297 HV) and 304 SS (231 HV) were substantially lower than the weld zone (900 HV). This is consistent with the microstructural observations described above. As FeTi and Fe_2Ti IMCs are known to be hard and brittle, the presence of numerous Fe-Ti IMCs in the weld zone leads to a significant increase in microhardness [12]. Moreover, the microhardness value of the weld zone showed a wide fluctuating range, varying from 760 HV to 1100 HV, indicating a poor uniformity of microhardness distribution. As for the joints with CoCrNi and CoCrNiFe fillers, the average microhardness values of NiTi and 304 SS were similar to those of the joints without filler. A distinct transitional area was observed between NiTi and the weld zone, with an average microhardness value of 422 HV with CoCrNi and 834 HV with CoCrNiFe. Comparing these two joints, it was noted that the transitional area in the joint with CoCrNi filler was narrower. This transitional area results from Ni-Fe and Cr-Ti compounds near the interface between NiTi and the weld zone. The average microhardness value of the weld zone was 290 HV with CoCrNi and 265 HV with CoCrNiFe, significantly lower than the joint without filler. This reduction in microhardness can be attributed to the suppression of Fe-Ti IMCs. Additionally, the fluctuation in microhardness value was much weaker, indicating a better uniformity of microhardness distribution in the weld zone.

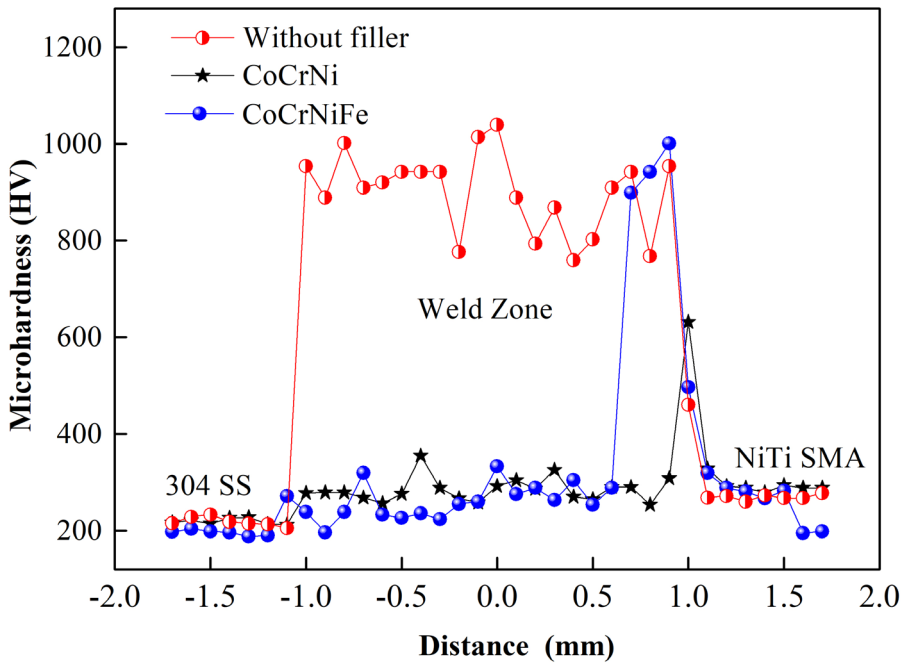

Fig. 11 Microhardness distribution of NiTi/304 SS lap joints with different fillers.

3.4 Tensile property

Fig. 12 illustrates the tensile shear properties of NiTi/304 SS lap joints with different fillers. Fractures occurred exclusively in the interface zone on the NiTi side, which is consistent with the results of cracking formation and microstructure characterization as cracks and IMCs were concentrated in this region. The joint without filler showed a tensile strength of 196±39 MPa. In contrast, the joints with CoCrNi and CoCrNiFe fillers exhibited a significantly enhanced tensile strength of 319±25 MPa and 377±33 MPa, respectively, which were 62.8% and 92.3% higher than that of the joint without filler. SEM images showing the fracture morphologies of NiTi/304 SS lap joints with different fillers are displayed in **Fig. 13**. In all three joints, a clear "river pattern" can be observed on the fractured surfaces, indicating a typical brittle fracture mode. The improved tensile properties can be attributed to two aspects. On the one hand, the effective restraint of initial cracking defects in the interface zone on the NiTi side, resulting from the suppression of brittle FeTi and Fe_2Ti IMCs, contributed to a higher tensile strength. On the other hand, the even distribution of microstructure reduced the stress concentration in the weld zone, leading to improved joint deformation uniformity [6].

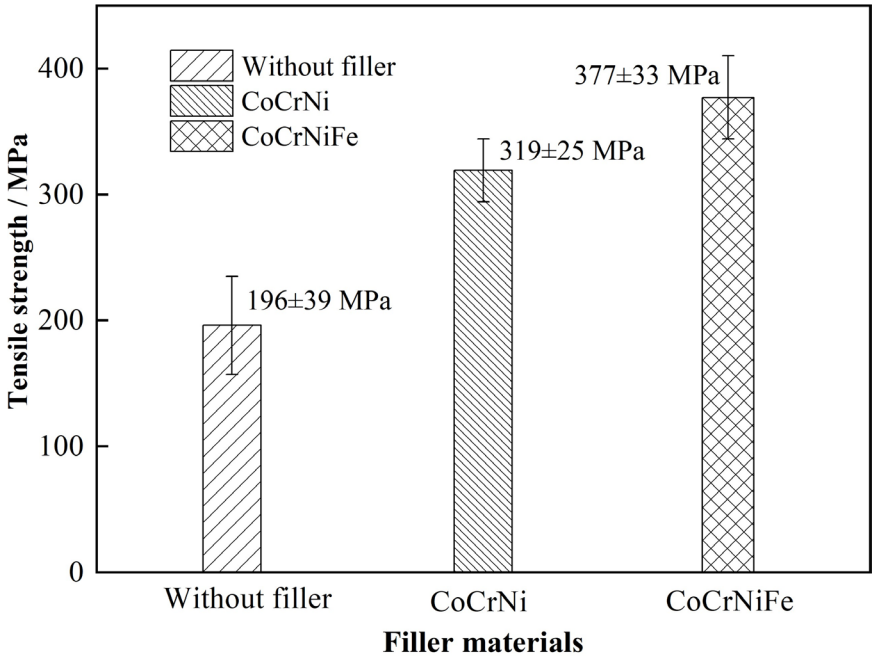

Fig. 12 Tensile shear properties of NiTi/304 SS lap joints with different fillers.

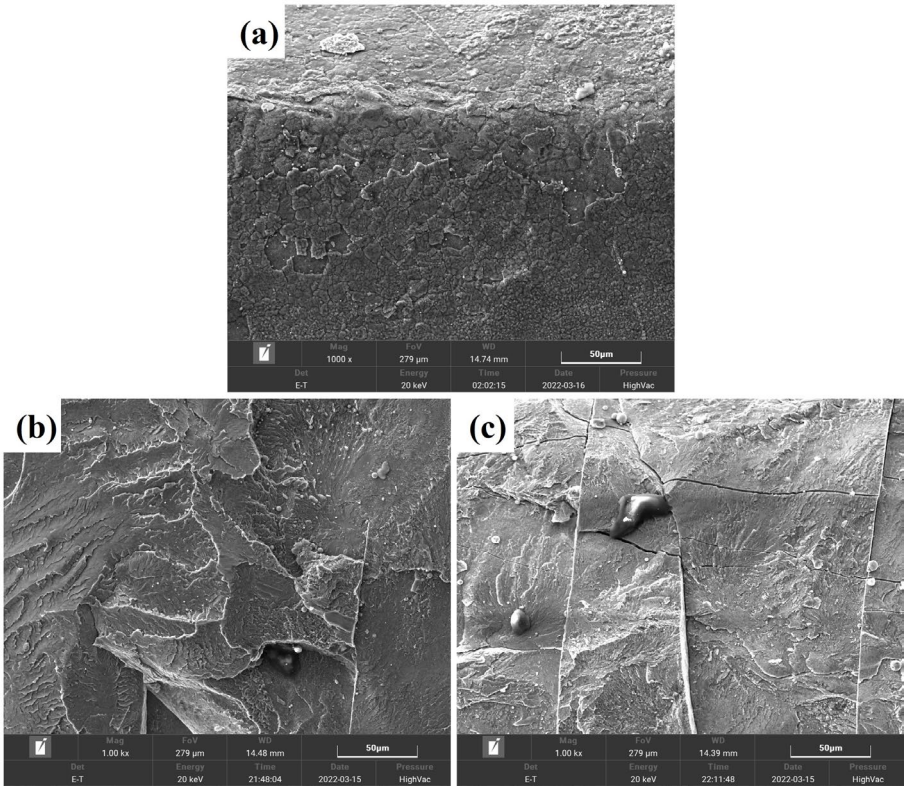

Fig. 13 Fracture morphologies of tensile specimens of NiTi/304 SS lap joints with different fillers.

(a): Without filler; (b): CoCrNi; (c) CoCrNiFe.

4. Conclusions

In this study, we investigated the microstructure and mechanical properties of laser-welded NiTi/304 SS lap joints using CoCrNi and CoCrNiFe filler materials and compared them with a self-fusing joint. The key findings can be summarized as follows:

(1) The interface zone on the NiTi side was identified as the weakest area regarding cracking defects in NiTi/304 SS lap joints. However, using CoCrNi and CoCrNiFe fillers effectively eliminated these cracking defects.

(2) CoCrNi and CoCrNiFe fillers demonstrated a significant ability to suppress the formation of FeTi and Fe_2Ti IMCs. Notably, the joint with CoCrNi filler exhibited a finer grain size and a lower density of LAGB compared to the joint with CoCrNiFe.

(3) The average microhardness value of the weld zone with CoCrNi and CoCrNiFe fillers was considerably lower than that observed in joints without filler, which is attributed to the significant suppression of FeTi and Fe_2Ti IMC formation. The joints with CoCrNi and CoCrNiFe exhibited a transitional area with higher microhardness values corresponding to the interface zone.

(4) Adding CoCrNi and CoCrNiFe fillers resulted in a substantial increase in tensile strength. The joint without filler showed a tensile strength of 196±39 MPa, while the joints with CoCrNi and CoCrNiFe fillers exhibited a tensile strength of 319±25 MPa and 377±33 MPa, respectively, indicating a significant enhancement in tensile properties.

Declaration of Competing Interest

The authors declared that they have no conflicts of interest in this work.

Author Contributions:

Conceptualization: Wang Yipeng, Zhang Dongni, and Li Hong; **Methodology:** Zhang Dongni, Li Hong, and Li Zhuoxin; **Analysis**: Wang Yipeng, Yang Zijia, Chen Xin and Cong Baoqiang. All authors have read and agreed to the published version of the manuscript.

Acknowledgments

This work was supported by Beijing Natural Science Foundation (No. 3232005), the National Natural Science Foundation of China (No. 52074017) and China-CEEC Joint Education Project for Higher Education (No. 2021113).

References

[1] K. Safaei *et al.*, “Additive Manufacturing of NiTi Shape Memory Alloy for Biomedical Applications: Review of the LPBF Process Ecosystem,” *Jom*, vol. 73, no. 12, pp. 3771–3786, 2021, doi: 10.1007/s11837-021-04937-y.

[2] N. Shayesteh Moghaddam *et al.*, “Achieving superelasticity in additively manufactured NiTi in compression without post-process heat treatment,” *Sci Rep*, vol. 9, no. 1, pp. 1–11, 2019, doi: 10.1038/s41598-018-36641-4.

[3] F. Du, L. Deng, X. Wang, M. Zhang, J. Jin, and J. Zhang, “Study on interfacial characteristics and properties of NiTi/Al–Mg joint by vaporizing foil actuator welding,” *Journal of Materials Research and Technology*, vol. 20, pp. 3429–3440, 2022, doi: 10.1016/j.jmrt.2022.08.090.

[4] J. Liu *et al.*, “Formation mechanism and control of welding cracks in dissimilar materials of Ni50Ti50 SMA and Ti-6Al-4V,” *J Manuf Process*, vol. 75, no. December 2021, pp. 552–564, 2022, doi: 10.1016/j.jmapro.2022.01.014.

[5] A. Chakraborty *et al.*, “Microstructures, wear and corrosion resistance of laser composite surfaced austenitic stainless steel (AISI 304 SS) with tungsten carbide,” *Opt Laser Technol*, vol. 134, no. September 2020, p. 106585, 2021, doi: 10.1016/j.optlastec.2020.106585.

[6] Y. Chen, S. Sun, T. Zhang, X. Zhou, and S. Li, “Effects of post-weld heat treatment on the microstructure and mechanical properties of laser-welded NiTi/304SS joint with Ni filler,” *Materials Science and Engineering A*, vol. 771, no. October 2019, p. 138545, 2020, doi: 10.1016/j.msea.2019.138545.

[7] S. S. Ao *et al.*, “Microstructure and mechanical properties of dissimilar NiTi and 304 stainless steel joints produced by ultrasonic welding,” *Ultrasonics*, vol. 121, no. December 2021, 2022, doi: 10.1016/j.ultras.2022.106684.

[8] Q. Li, Y. Zhu, and J. Guo, “Microstructure and mechanical properties of resistance-welded NiTi/stainless steel joints,” *J Mater Process Technol*, vol. 249, no. January, pp. 538–548, 2017, doi: 10.1016/j.jmatprotec.2017.07.001.

[9] M. J. C. Oliveira, R. H. F. Melo, T. M. Maciel, and C. J. de Araújo, “Microstructural evaluation and mechanical behaviour of dissimilar niti-stainless steel joints welded by micro gas tungsten arc welding,” *Mater Chem Phys*, vol. 224, no. March 2017, pp. 137–147, 2019, doi: 10.1016/j.matchemphys.2018.12.013.

[10] H. Niu, H. C. Jiang, M. J. Zhao, and L. J. Rong, “Effect of interlayer addition on microstructure and mechanical properties of NiTi/stainless steel joint by electron beam welding,” *J Mater Sci Technol*, vol. 61, 2021, doi: 10.1016/j.jmst.2020.05.043.

[11] K. Zhang, P. Peng, and Y. N. Zhou, “Laser welding-brazing of NiTi/304 stainless steel wires with beam defocus and large offset,” *Materials Science and Engineering A*, vol. 835, no. October 2021, p. 142660, 2022, doi: 10.1016/j.msea.2022.142660.

[12] A. Shamsolhodaei, J. P. Oliveira, N. Schell, E. Maawad, B. Panton, and Y. N. Zhou, “Controlling intermetallic compounds formation during laser welding of NiTi to 316L stainless steel,” *Intermetallics (Barking)*, vol. 116, 2020, doi: 10.1016/j.intermet.2019.106656.

[13] C. H. Ng, E. S. H. Mok, and H. C. Man, “Effect of Ta interlayer on laser welding of NiTi to AISI 316L stainless steel,” *J Mater Process Technol*, vol. 226, pp. 69–77, 2015, doi: 10.1016/j.jmatprotec.2015.06.039.

[14] A. Shojaei Zoeram, A. Rahmani, and S. A. A. Akbari Mousavi, “Microstructure and properties analysis of laser-welded Ni–Ti and 316l sheets using copper interlayer,” *J Manuf Process*, vol. 26, pp. 355–363, 2017, doi: 10.1016/j.jmapro.2017.02.005.

[15] H. Li, D. Sun, X. Cai, P. Dong, and X. Gu, “Laser welding of TiNi shape memory alloy and stainless steel using Co filler metal,” *Opt Laser Technol*, vol. 45, no. 1, pp. 453–460, 2013, doi: 10.1016/j.optlastec.2012.06.010.

[16] S. Asadi, T. Saeid, A. Valanezhad, I. Watanabe, and J. Khalil-Allafi, “Effects of Ni powder addition on microstructure and mechanical properties of NiTi to AISI 304 stainless steel archwire dissimilar laser welds,” *J Manuf Process*, vol. 55, no. April, pp. 13–21, 2020, doi: 10.1016/j.jmapro.2020.03.041.

[17] Y. Chen, S. Sun, T. Zhang, X. Zhou, and S. Li, “Effects of post-weld heat treatment on the microstructure and mechanical properties of laser-welded NiTi/304SS joint with Ni filler,” *Materials Science and Engineering: A*, vol. 771, 2020, doi: 10.1016/j.msea.2019.138545.

[18] S. Yan, H. Zhou, Z. Zhu, Y. Fu, and J. Tian, “High strength-ductility synergy in a laser welded dissimilar joint of CrCoNi medium-entropy alloy and stainless steel,” *Materials Science and Engineering: A*, vol. 840, 2022, doi: 10.1016/j.msea.2022.142854.

[19] G. Wang *et al.*, “Mechanical properties and microstructure evolution of CrMnFeCoNi HEA/304 SS dissimilar brazing joints,” *J Alloys Compd*, vol. 829, p. 154520, 2020, doi: 10.1016/j.jallcom.2020.154520.

[20] Y. Zhang *et al.*, “Research and development of welding methods and welding mechanism of high-entropy alloys: A review,” *Mater Today Commun*, vol. 28, no. June, p. 102503, 2021, doi: 10.1016/j.mtcomm.2021.102503.

[21] S. Park, H. Nam, J. Park, Y. Na, H. Kim, and N. Kang, “Superior-tensile property of CoCrFeMnNi alloys achieved using friction-stir welding for cryogenic applications,” *Materials Science and Engineering A*, vol. 788, no. March, p. 139547, 2020, doi: 10.1016/j.msea.2020.139547.

[22] H. Azhari-Saray, M. Sarkari-Khorrami, A. Nademi-Babahadi, and S. F. Kashani-Bozorg, “Dissimilar resistance spot welding of 6061-T6 aluminum alloy/St-12 carbon steel using a high entropy alloy interlayer,” *Intermetallics (Barking)*, vol. 124, 2020, doi: 10.1016/j.intermet.2020.106876.

[23] X. Gu and L. Zhang, “Laser lap welding of TC4 titanium alloy to 6082 aluminum alloy using a CoNiCuNb0.5 V1.5 high entropy alloy filler,” *Mater Lett*, vol. 312, 2022, doi: 10.1016/j.matlet.2021.131562.

[24] J. Zhou *et al.*, “Dissimilar laser lap welding of Mg and Al alloys using a CoCrFeNi medium-entropy alloy interlayer,” *Opt Laser Technol*, vol. 157, 2023, doi: 10.1016/j.optlastec.2022.108639.

[25] D. Liu, W. Wang, X. Zha, R. Guo, H. Jiao, and L. Zhao, “Effects of groove on the microstructure and mechanical properties of dissimilar steel welded joints by using high-entropy filler metals,” *Journal of Materials Research and Technology*, vol. 13, 2021, doi: 10.1016/j.jmrt.2021.04.060.

[26] H. Wang, J. Xie, Y. Chen, W. Liu, and W. Zhong, “Effect of CoCrFeNiMn high entropy alloy interlayer on microstructure and mechanical properties of laser-welded NiTi/304 SS joint,” *Journal of Materials Research and Technology*, vol. 18, pp. 1028–1037, May 2022, doi: 10.1016/j.jmrt.2022.03.022.

[27] Y. Hu, Y. Niu, Y. Zhao, W. Yang, X. Ma, and J. Li, “Friction stir welding of CoCrNi medium-entropy alloy: Recrystallization behaviour and strengthening mechanism,” *Materials Science and Engineering A*, vol. 848, Jul. 2022, doi: 10.1016/j.msea.2022.143361.

[28] D. G. Shaysultanov, G. A. Salishchev, Y. V. Ivanisenko, S. V. Zherebtsov, M. A. Tikhonovsky, and N. D. Stepanov, “Novel Fe36Mn21Cr18Ni15Al10high entropy alloy with bcc/B2 dual-phase structure,” *J Alloys Compd*, vol. 705, pp. 756–763, 2017, doi: 10.1016/j.jallcom.2017.02.211.

[29] H. Li, Y. Li, Y. Nie, and S. Yan, “Small-scale mechanical properties and deformation mechanisms of a laser welded CrCoNi medium-entropy alloy joint,” *Materials Science and Engineering A*, vol. 855, Oct. 2022, doi: 10.1016/j.msea.2022.143959.

[30] H. Li, Y. Li, Y. Nie, and S. Yan, “Small-scale mechanical properties and deformation mechanisms of a laser welded CrCoNi medium-entropy alloy joint,” *Materials Science and Engineering A*, vol. 855, Oct. 2022, doi: 10.1016/j.msea.2022.143959.

[31] G. Laplanche, A. Kostka, O. M. Horst, G. Eggeler, and E. P. George, “Microstructure evolution and critical stress for twinning in the CrMnFeCoNi high-entropy alloy,” *Acta Mater*, vol. 118, pp. 152–163, Oct. 2016, doi: 10.1016/j.actamat.2016.07.038.

[32] Y. Lu *et al.*, “Investigation of microstructure, texture, and mechanical properties of FeCoNiCrMn high entropy alloy during drive friction welding,” *Mater Charact*, vol. 189, no. May, p. 111959, 2022, doi: 10.1016/j.matchar.2022.111959.

https://dspace.org/

Enhancing microstructural and mechanical characteristics of laser welded NiTi SMA/304 SS lap joints with medium and high entropy alloy fillers

Wang, Yipeng; Zhang, Dongni; Li, Hong; Li, Zhuoxin; Yang, Zijia ...

2024-06-01
Springer
https://doi.org/10.1007/s40194-023-01668-3
Wang Y, Zhang D, Li H, et al., (2024) Enhancing microstructural and mechanical characteristics of laser welded NiTi SMA/304 SS lap joints with medium and high entropy alloy fillers. Welding in the World, Volume 68, June 2024, pp. 1389-1399

Downloaded from a DSpace repository. https://dspace.org/